RELATIONSHIPS BETWEEN COHERENT STRUCTURE AND TURBULENT STATISTICS STRUCTURE IN WIND-DRIVEN TURBULENT FLOW, VIA DNS

Tomoaki Kunugi
Dept of Nuclear Eng., Kyoto University
Yoshida, Sakyo, Kyoto, 606-8501, JAPAN
kunugi@nucleng.kyoto-u.ac.jp

Shin-ichi Satake
Dept. of Mech. Intellectual Sys. Eng., Toyama Univ.
3190 Gofuku, Toyama city, Toyama,
930-8555, JAPA N
ssatake@eng.toyama-u.ac.jp

Yoshinobu Yamamoto
Dept of Nuclear Eng., Kyoto University
yyama@nucleng.kyoto-u.ac.jp

Akimi Serizawa
Dept of Nuclear Eng., Kyoto University
serizawa@nucleng.kyoto-u.ac.jp

ABSTRACT

In this study, direct numerical solution procedure (MARS method) for a coupled gas-liquid flow is employed to investigate the relationships between the coherent structure and turbulent statistics in wind-driven turbulent flow. The Reynolds number is about 3540 based on the gas layer height and the free stream velocity. As the results, near free-surface, like a viscous sublayer structure cannot be observed, turbulent was constrained and gas flow was laminarized compared with the smooth wall boundary flow. But, vertical fluctuation component is lager than that of no-deformation free-surface flow and turbulent intensities show the isotropy tendency. In the present condition, turbulent structure near free-surface is like an incompletely or completely rough bed wall structure. In the concentration fileds, near free-surface in the gas side, alternating high and low consentlation streaks existed as well as velocity fileds and high concentration regions at the free-surface are observed in the regions where high pressure existed and free-surfaces were deformed toward the downward. These mean that the effects of the surface deformation are dominant the mass transfer accross the free-surface in capillary wave of the wind-driven turbulent flow.

INTRODUCTION

Free-surface turbulent flows are very often found in the industrial devices such as a nuclear fusion reactor and a chemical plant, not to speak of those in river and ocean. Therefore, to investigate the turbulent structures near free-surface is very important to understand the heat and mass transport phenomena across the free surface and an appropriate of any turbulence model for heat and mass transfer across the free-surface is strongly requested for engineering. The dominant factors of heat and mass transfer across the free-surface are considered the effects of (a) the high Prandtl or Schmidt number fluid, (b) buoyancy (c) surfactant and such as (d) surface deformation. Furthermore, by the free-surface behaviors, free-surface turbulent flows would be divided into the three situations; (1) rigid-lid, (2) ripples and (3) breaking status. Figure 1 shows this categorization of free-surface turbulent flows. In general, the combination of them greatly impacted on turbulent heat and mass transfer, but its complex process and mechanism haven't been understood well. As for (1) rigid-lid status, some experimental or numerical studies with scalar transport including a buoyancy effect were carried out [1]-[7]. The interesting information about the relationship between turbulent motion, so-called "surface renewal vortex", and the scalar transport, and also the interaction between buoyancy and turbulence were obtained. However, in case of the capillary and capillary-gravity range wind velocity, i.e., around 2-7m/s, the turbulent characteristics near the free-surface could be influenced by a deformation of the free-surface due to the wind shear. These like, the accuracy near free-surface experimental or DNS (Direct Numerical Simulation) database haven't been enough to make any turbulence model near free-surface until now, especially considered the surface deformation, high Prandtl number fluid, and buoyancy effects.

The aim of this study is to investigate the relathionships betwen coherent structure and turbulent statistics of the free-surface in open-channel flow deformed by the wind shear, by means of direct numerical solution procedure for a coupled gas-liquid flow, i.e., MARS (Multi-Interfaces Advection and Reconstruction slover) method [8].

NUMERICAL PROCEDURE

Since the treatment of multiphase flows in the MARS method is based on a volume fraction function $F\ (t,\ x_i\ )$, the spatial distribution of each material $F\ (t, x_i\ )$ can be defined as:

$$\langle F \rangle = \sum F_m = 1.0 \qquad (1)$$

Here, F_m denotes a volume fraction of m-th fluid and $< >$ represents a spatial mean.

In the present study, the following assumptions for deriving the governmental equations are made: 1) Newtonian fluid is assumed, 2) thermal properties are kept to be constant and 3) thermal radiation and

viscous dissipation are neglected. The continuity equation for the multiphase flows of m fluids can be expressed as:

$$\frac{\partial F_m}{\partial t}+(U\cdot\nabla)F_m = \frac{\partial F_m}{\partial t}+\nabla\cdot(F_m U)-(F_m\cdot\nabla)U=0 \quad (2)$$

The momentum equation with the CSF (Continuum Surface Force) model proposed by Brackbill [9] can be written by

$$\frac{\partial U}{\partial t}+\nabla(UU) = G-\frac{1}{\langle\rho\rangle}\nabla P-\nabla\cdot\tau+\frac{1}{\langle\rho\rangle}F_V \quad (3)$$

The CSF term, F_v at the certain surface position x_s, can be modeled as:

$$F_V(x_s)=\left[\sigma\kappa(x_s)+\tau_2(x_s)_{ii}-\tau_1(x_s)_{ii}\right]n(x_s)\langle\rho(x_s)\rangle/\bar{\rho} \quad (4)$$

where, σ is a surface tension coefficient, $\kappa(x_s)$ is surface curvature at x_s and n is normal vector to the surface at x_s. Other thermal properties, such as the mean density ρ the viscosity μ and the viscous stress τ are defined by the following equations,

$$\left.\begin{aligned}\langle\rho\rangle&=\sum(F_m\rho_m),\quad \bar{\rho}=(\rho_g+\rho_l)/2\\ \langle\langle\mu\rangle\rangle&=\left[\begin{aligned}&\phi_g\times\left\{sign\left(F_g-F_l\right)+1\right\}\\&+\phi_l\times\left\{1-sign\left(F_g-F_l\right)\right\}\end{aligned}\right]/2\\ \tau&=-\left[\langle\langle\mu\rangle\rangle/\langle\langle\rho\rangle\rangle\right]\left[(\nabla U)+(\nabla U)^T\right]\end{aligned}\right\} \quad (5)$$

here, the suffices, g and l, denote the gas and the liquid phases, respectively. ϕ is a general variable such as ρ and μ. Another average of properties at the free surface region is defined as, $<<\phi>>$.

The momentum equation (3) can be solved by means of the well-known projection method [10].

Once the velocity field can be obtained, the fluid volume flux can be transported by using Eq. (2) with the MARS method.

The mass transport equation for the carbon-dioxide gas can be expressed as follows:

$$\frac{\partial}{\partial t}\langle\rho\rangle C+\nabla\cdot(\langle\rho\rangle CU)=\nabla\cdot(D_m\nabla C)+S \quad (6)$$

where, C is a concentration, D_m is a molecular diffusivity and S is an absorbed mass flux at the free-surface based on the following Henry's law;

$$C_s = P_s/H, \quad (7)$$

here C_s is a concentration at free-surface corresponding to the saturation solubility, P_s is an instantaneous pressure at free surface and H is the Henry's constant corresponding to the pressure.

As for the discretization of the governing equations on the Cartesian coordinate system, the second-order scheme for the spatial differencing terms is used on the staggered grid system and the Euler implicit scheme is used for the first stage of projection method to solve the momentum equation. The gas absorption term is treated as an internal boundary condition based on Eq.(7) in the computation program.

COMPUTATIONAL CONDITIONS

The physical problem treated here is the motion of two Newtonian incompressible fluids allowed the deformation of the interface problem between them. In Fig.2, the schematic view is shown. Both gas and liquid flows flow in parallel. The computational domain is L_x=0.25 m in length (x-direction), L_y=2h=0.05 m in height (y-direction) and L_z=0.125 m in width (z-direction), where h denotes the gas layer height. The periodic boundary conditions in the spanwise (x) and streamwise (z) directions are imposed, the free-slip condition is applied to upper gas boundary and no-slip condition is imposed lower water boundary. The free stream velocity in gas phase is about 2.2 m/s and Reynolds number based on the gas layer height(h) and the free stream velocity V_{top} is $Re(=V_{top}h/\nu)$=3540. The number of the computational grids is 128 in x-direction (streamwise), 216 in y-direction (height) and 128 in z-direction (spanwise).

RESULTS AND DISCUSSION

Figures 3 and 4 show the profiles of mean velocity and the gas-side turbulent intensity. Compared with the smooth wall turbulent boundary layer flow, laminarized gas-flow drags water flow like a Couette flow. Near the bottom wall flow doesn't be influenced by the gas-flow motion because the water depth is enogh large. In the deformed free-surface turbulent flow, vertical component of the turbulent intensity near free-surface has a significant value as well as the spanwise one. The turbulent intensity peaks are different from the others. This may indicate that the vertical component of the turbulent intensity is mainly from the wave motion, the streamwise one is mainly from bulk turbulent boundary layer of the gas-flow, and the both effects interact on the spanwise one.

Figures 5 (a) and (b) show the free-surface behaviors and the iso-surfaces of the instantaneous high pressure; Instantaneous free-surface behaviors

as shown in Fig.5 (a), top view and near free-surface, the iso-surface of the instantaneous high pressure as shown in Fig.5 (b). Three-dimensional capillary wave motion can be observed in Fig.5 (a). In the present condition, any wave-breaking and droplet formation cannot be observed. Upper part of the free-surface, high pressure streaks stretched to spanwise direction can be seen in Fig.5 (b). This might imply that statistical surface deformation were two-dimensional one. In these high pressure regions, free-surfaces were deformed toward the downward. This is the reason why the pressure difference and surface tension are balanced in the deformed free-surface.

Figure 6 shows the iso-surfaces of instantaneous high streamwise velocity components near free-surface. In both gas and water sides, the streaks stretched to streamwise direction can be seen, as well as a buffer layer turbulence structure near solid wall, and the water-side streaks underneath the free-surface seems to be driven by the gas-side streaks. This indicates that turbulent structure near free-surface in wind-driven turbulent flow is not like a mixing layer structure but a wall turbulence structure. These features are similar to the non-deformed gas-liquid turbulent flow [7]. However, in the deformed free-surface flow, the surface deformation and the streak structure which is the one of the most notable coherent structures of a turbulent flow near wall-boundary seem to influence with each other. Thus, wave motion from the sweep like gas-flow seems to break the streak structure and disturb self-sustaining process which is the quasi-cyclic process passing quiescent and activated period in turn [11]. Consequently, like a viscous sublayer structure cannot be observed near free-surface, turbulent was constrained and gas flow was laminarized compared with the smooth wall boundary flow. Vertical fluctuation component is lager than that of the no-deformation flow, turbulent intensities show the isotropy tendency. In the present condition, near free-surface turbulent structure is like an incompletely or completely rough bed wall structure. Visualizations of these coherent structures in wind-driven turbulent flow are shown in Fig. 7.

Figures 8 (a)-(c) show the contours of the instantaneous concentration fields. Near free-surface in the gas side, alternating high and low consentlation streaks are observed in Fig 8 (b). In Fig.8 (a), high concsntration regions are observed in the regions where high pressure existed and free-surfaces were deformed toward the downward at the free-surface. These indicate that the bulk mass transfer is conducted throught the turbulent structures in the gas side and the effects of the free-surfacee deformations on the mass transfer accross the free-surface played the dominant role.

SUMMARY

In this study, DNS is employed to investigate the relationships between the coherent structure and turbulent statistics in wind-driven turbulent flow. As the follwing results are obtained;

(1) Near free-surface, alternating high and low speed streaks are observed in both gas and water side and the water-side streaks seems to be driven by gas-side streaks as well as no-deformation gas-liquid flow.

(2) In the deformed free-surface flow, the surface deformation and the streak structures seem to influence each other. Vertical fluctuation component is lager than that of no-deformation free-surface flow and turbulent intensities show the isotropy tendency. Like a viscous sublayer structure near free-surface, cannot be observed, turbulent was constrained and gas flow was laminarized compared with the smooth wall boundary flow. In the present condition, turbulent structure near free-surface is like an incompletely or completely rough bed wall structure.

(3) Alternating high and low consentlation streaks existed near free-surface in the gas side and high concsntration regions are observed in the at the free-surface regions where high pressure existed and free-surfaces were deformed toward the downward. These indicate that the bulk mass transfer is conducted throught the turbulent structures in the gas side and the mass transfer accross the free-surface is conducted throuth the surface deformation.

Acknowledgments

This work was supported by ACT-JST* and Japan Atomic Energy Research Institute (JAERI).

* " Research and development applying advanced computational science and technology " of Japan Science and Technology Corporation

References

[1] Nagaosa, R. and Saito, T., AIChE J., vol. 43, 2393, 1997.

[2] Handler et al, *Phys. Fluids*,11, 2607, 1999.

[3] Komori et al., Int. J. Heat Mass Transfer, 25, 513, 1982.

[4] Rashidi, M. and Banerjee, S., *Phys. Fluids*, 31, 2491, 1988.

[5] Komori, S., Murakami, Y. and Ueda, H., *J. Fluid Mech.*, 203, 103, 1989.

[6] Lombardi, P., Angelis, V. D., Banerjee, S., *Phys. Fluids*, 8, 1643, 1996.

[7] Angelis, V. D. and Banerjee, S., *Turbulence and Shear Flow Phenomena-1*, Edited by Banerjee S. and Eaton, J. K., Begell House Inc., 1249, 1999.

[8] Kunugi, T, *Trans. JSME Ser. B*, 63, 1576, 1997.[in Japanese]; ibid, *Proc. ISAC 97 High Performance Computing on Multiphase Flows*, JSME Centennial Grand Congress, 25, 1997.

[9] Brackbill, J. U., Kothe, D. B. and Zemach, C., *J. Comput. Phys.*, 100, 335, 1992.

[10] Chorin, A. J., *Math. of Comput.*, 22, 745, 1968.

[11] Jimenez, J.M. and Moin. P., *J.Fluid Mech.*, 225, 213.1991.

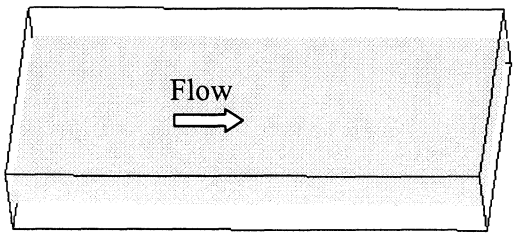

(1) Rigid-lid status, for example, sub-critical open-channel flow at low Froude or Reynolds number etc.
This figure shows the free-surface behavior of a sub-critical turbulent open-channel flow.

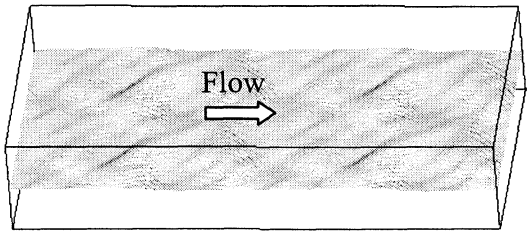

(2) Ripples status, for example, critical or super-critical open-channel flow, wind-driven turbulent flow, shallow or deepwater wave, etc.
This figure shows the free-surface behavior of a super-critical turbulent open-channel flow.

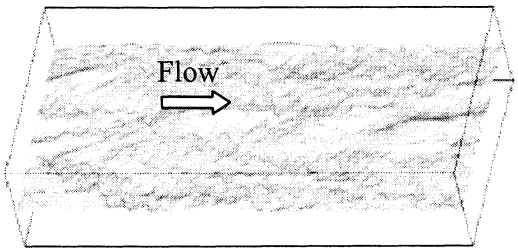

(3) Breaking status, for example, wind-driven turbulent flow, shallow or deepwater wave, etc.
This figure shows the free-surface behavior of a wind-driven turbulent flow.

Fig.1 Categorization of free-surface turbulent flows by the free-surface behaviors

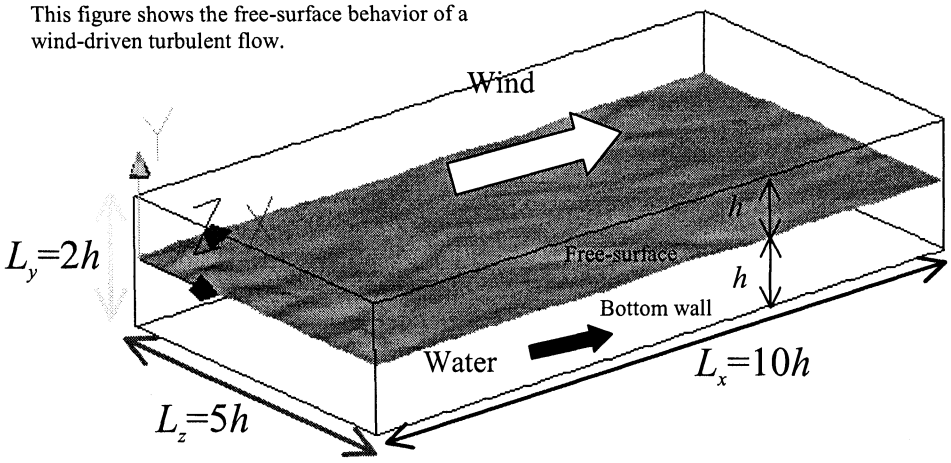

Fig.2 Computational domain and coordinate system

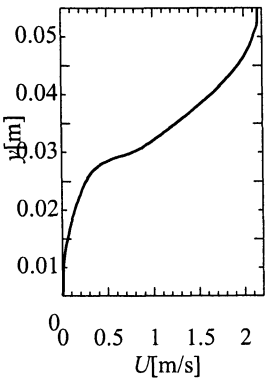

Fig.3 Mean velocity profile

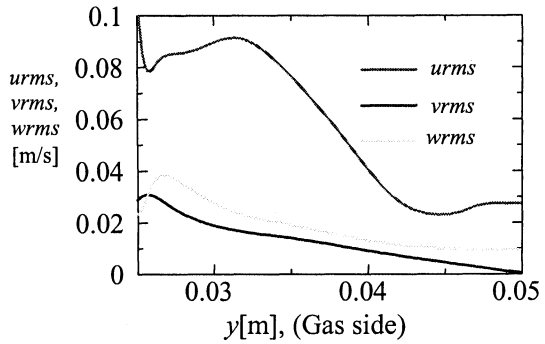

Fig.4 Turbulent intensity profiles

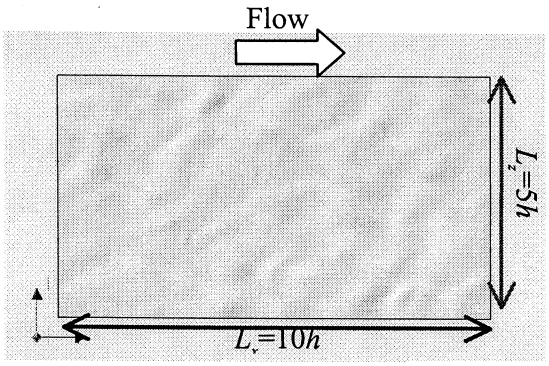

Fig. 5 (a) Top view of the instantaneous free-surface behaviors

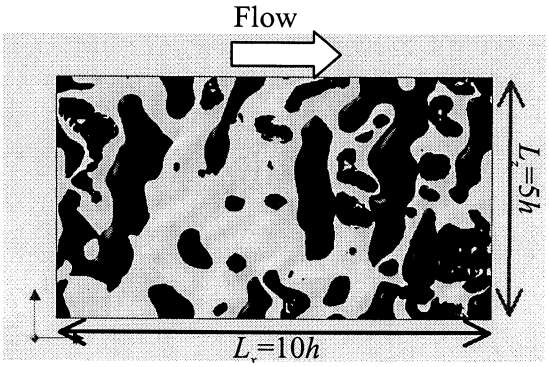

Fig. 5 (b) Top view of the instantaneous high pressure iso-surface
Dark blue color corresponds to atmospheric pressure region.

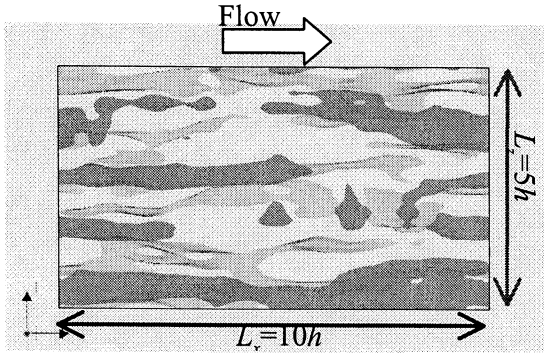

Fig. 6 Top view of the instantaneous high streamwise velocity components near free-surface
U=1.15 [m/s] gas-side (Brown region), U=0.45 [m/s] water-side (Light blue)

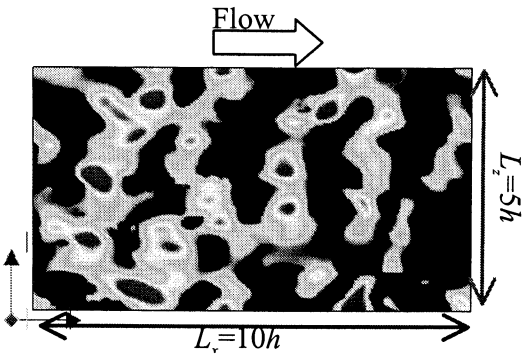

Fig. 8 (a) contour of the instantaneous consentration field at the free-surface (Top view)
0.01(Blue)< C<0.18(Red)

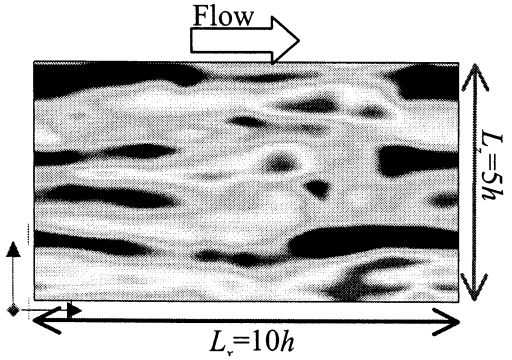

Fig. 8 (b) contour of the instantaneous consentration field near the free-surface (Top view)
0.2(Blue)< C<0.5(Red)

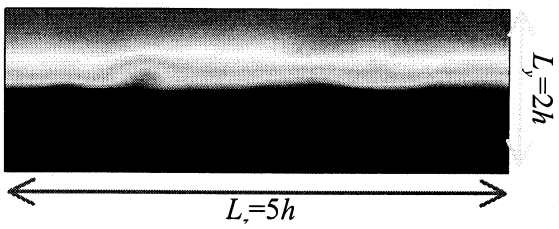

Fig. 8 (c) contour of the instantaneous consentration field (End view)
0.0(Blue)< C<1.0(Red)

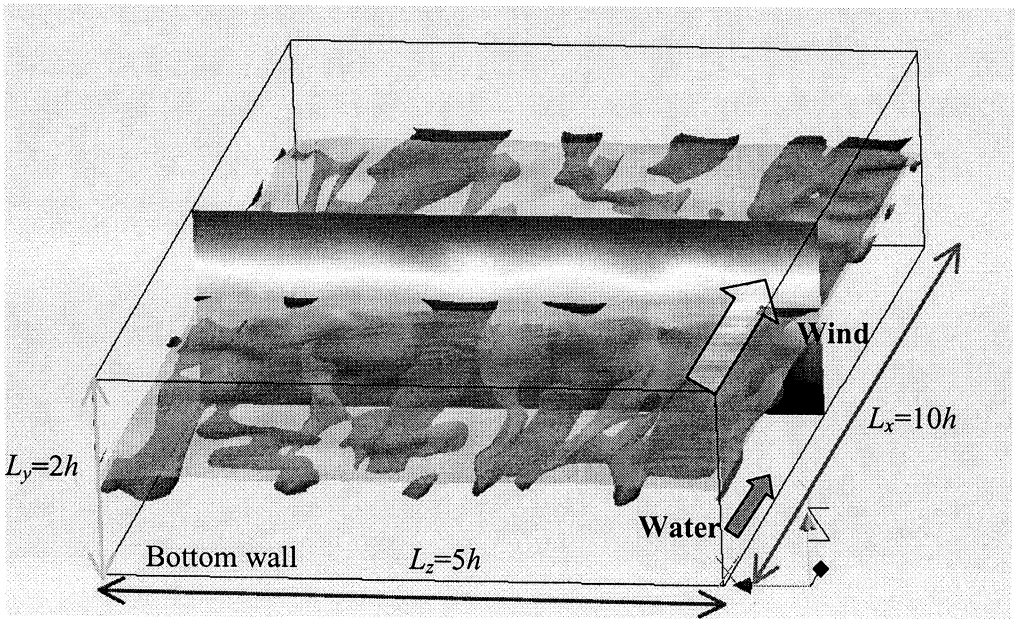

Fig. 8 (a) Bird view from the gas-side of the instantaneous high streamwise velocity components near free-surface
U=1.15 [m/s] gas-side (Brown region), U=0.45 [m/s] water-side (Light blue region)
Color contour shows streamwise instantaneous velocity U (-0.01[m/s] Blue<U<2.24[m/s] Red)

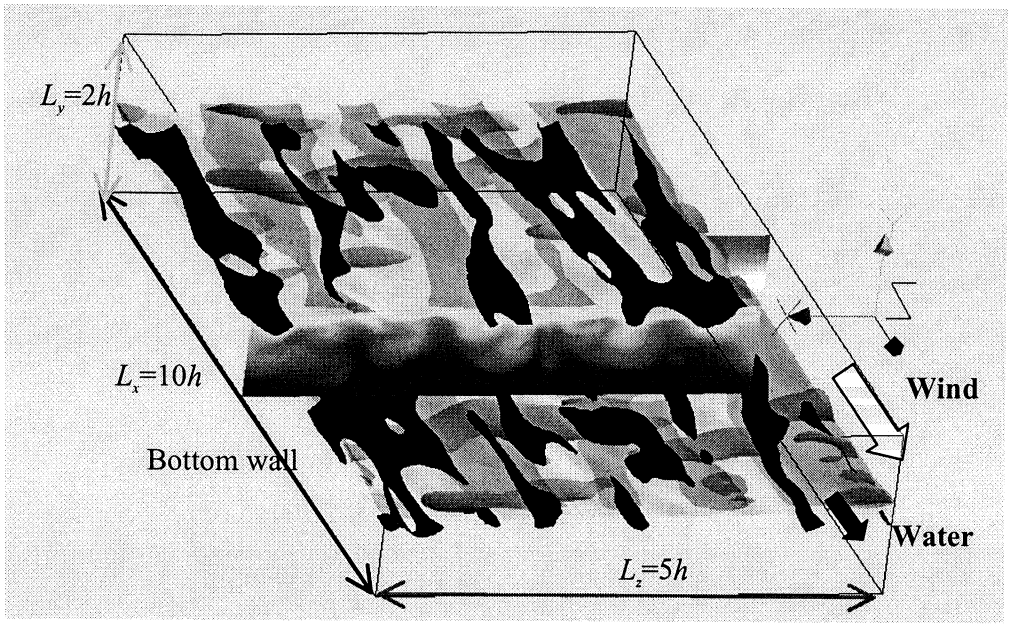

Fig. 8 (b) Bird view from the water-side of the instantaneous high streamwise velocity components near free-surface
U=1.15 [m/s] gas-side (Brown region), U=0.45 [m/s] water-side (Light blue region)
Color contour shows streamwise instantaneous velocity U (-0.01[m/s] Blue<U<2.24[m/s] Red)